PHYSICS AND CHEMISTRY OF SOLID STATE
V. 26, No.4 (2025) pp. 912-922
Section: Chemistry

DOI: 10.15330/pcss.26.4.912-922

Vasyl Stefanyk Carpathian National University

ФІЗИКА І ХІМІЯ ТВЕРДОГО ТІЛА
Т. 26, № 4 (2025) С. 912-922
Хімічні науки

UDC: 542.957:547.7:547.854

ISSN 1729-4428 (Print)
ISSN 2309-8589 (Online)

A.I. Rustamova[1], L.V. Huseynova[2], S.N. Osmanova[1,3], V.M. Ahmadov[1], E.H. Ismailov[1]

Impact of Thermal Reduction in an H_2 Stream on the Composition of Ferrocene Degradation Products

[1]*Institute of Catalysis and Inorganic Chemistry, Baku, Azerbaijan,*
[2]*Azerbaijan State Oil and Industry University, Baku, Azerbaijan*
[3]*Khazar University, Baku, Azerbaijan, sevinj.nasib.osmanli.26@gmail.com*

The gas-phase and solid products formed during the thermal reduction of ferrocene in a hydrogen flow in the temperature range of 373–1073 K were investigated. The identified gas-phase products include methane, ethane, propane, butane, *n*-pentane, *n*-hexane, and cyclopentadiene, while the solid products consist of nanosized particles of iron and carbon. The temperature dependences of the concentrations of the detected gas-phase products were obtained. It was shown that the formation of iron nanoparticles during the thermal decomposition of ferrocene in a hydrogen atmosphere proceeds with the simultaneous formation of metallic iron, iron carbide, and amorphous carbon. Their relative contents in the solid residue strongly depend on the reaction conditions. The nucleation process under hydrogen atmospheres occurs with the formation of smaller nuclei, which promotes a more intense formation and growth of nanoparticles. The composition of the solid residues can be controlled by varying the experimental parameters, such as reaction time, temperature, and iron precursor concentration. The magnetic properties of the resulting solid products may also be tuned through modulation of particle structure and phase composition.

Keywords: ferrocene, thermal reduction, gas-phase, solid phase products, iron, iron carbide nanoparticles, XRD, FMR.

Received 07 January 2025; Accepted 12 November 2025.

Introduction

Since its discovery in the 1950s [1, 2], the metallocene ferrocene ($Fe(Cp)_2$) has become a widely studied compound due to its unique properties [3, 4]. This classic sandwich complex, in which two cyclopentadienyl ligands are attached to a central iron core, is characterized by a relatively high vapor pressure at moderate temperatures, it is non-toxic and stable in air at room temperature and, therefore, is an easy-to-handle precursor for the synthesis of functional materials [5, 6]. In particular, the application of ferrocene in the preparation of iron-containing thin films for optoelectronic devices [7, 8] or iron thin films in an oxidizing atmosphere [9] has been successfully established. Thermal decomposition of $Fe(Cp)_2$ can form iron nanoparticles (NPs), which can be used as functional nanomaterials for energy conversion and storage systems [10, 11]. The iron released during the decomposition of ferrocene can be deposited as nanoparticles, which can be used as catalysts for chemical reactions or as components for magnetic nanomaterials. At sufficiently high temperatures and under suitable conditions, the released iron can act as a catalyst for the formation of carbon nanomaterials such as carbon nanotubes or carbon nanoparticles [12, 13]. Iron from ferrocene catalyzes the decomposition of hydrocarbons to release pure carbon, which is then deposited on the iron surface as nanotubes or particles [14]. Iron nanoparticles have been of great interest to researchers over the past few decades due to their wide range of applications including data storage, environmental remediation, catalysis, and disease diagnosis and therapy. Among them, iron oxides and

metallic iron have been widely studied [15, 16]. Although iron oxides are non–toxic and stable in air/biological environments, their magnetization is low, especially at the nanoscale. Iron nanoparticles are easily oxidized to form Fe_2O_3. By passivating the surface of iron nanoparticles, core/shell structures are created and thus stabilize these nanoparticles [17, 18].

Ferrocene decomposition in an oxidative, reductive and inert gas atmosphere occurs at a temperature of 673-1073 K [19–21]. Pyrolysis of ferrocene begins to decompose with the release of hydrocarbon molecules, solid carbon and iron particles. In the presence of hydrogen, these hydrocarbons and solid carbon can additionally react to form products such as methane, ethane, or other low-molecular hydrocarbons [22, 23].

This paper presents the results of a study of the thermal reduction of ferrocene in a hydrogen stream in the range of 373–1073 K, gas-phase reaction products using on-line gas chromatography and microreactor coupled to a mass spectrometer, and solid reaction products using X-ray diffractometry and ferromagnetic resonance.

I. Experimental part

The reduction process was carried out under the conditions described below: 0.3 g of pre-prepared, highly dispersed ferrocene was poured into a reactor tube placed in a thermostatic furnace equipped with an electric heater between two layers of quartz grains, and the reaction was carried out in a continuous mode. To determine the reaction temperature, a thermocouple was placed in the center of the catalyst layer, and the temperature was controlled by a Micromax microelectronic controller. The reduction process in the temperature range of 373–1073 K, H_2 at a rate of 15 ml/min was carried out at a volume rate. The reaction products were analyzed online using an Agilent 7820A GC gas chromatograph equipped with a ZB-624 capillary column 30 m long and 0.53 mm internal diameter with an FID detector. The schematic diagram of the experimental laboratory setup used for the ferrocene reduction reaction is shown in Figure 1.

The parameters of analysis performed on the gas chromatograph with flame ionization detector Agilent 7820A are set as follows: Helium flow rate – 15 ml/min; Air flow rate – 300 ml/min; Hydrogen flow rate – 30 ml/min; Detector temperature – 573 K, Inlet temperature – 523 K; Inlet pressure – 1.2606 psi; Furnace temperature – 313-453K; ZB-624 capillary cable length – 30 m; diameter 0.53 mm; Helium pressure in the capillary tube – 1.2606 psi.

Integrated microreactor-mass-spectrometer system made by Hiden Analytical, UK and installed in April 2022 at the Institute of Catalysis and Inorganic Chemistry is used for determination of its pyrolysis. This system allowed to carry out the on line measurements up to 1173 K, to identify the gas-phase reaction products - H_2, N_2, CH_4, C_2H_4, C_2H_6, C_3H_6, C_3H_8, C_2H_2.

The formation of the above gas-phase and solid products was confirmed by X-ray diffraction methods using a diffractometer XRD D2 EPR_{mikro} spectrometer from Bruker, Germany, a mass spectrometer coupled to a microreactor Catlab, Hiden Analytical, UK and a chromatograph GC 7280 from Agilent.

II. Results and discussion

Table 1 shows the results of chromatographic and mass-spectrometric analysis of gas-phase products of thermal decomposition of ferrocene in a hydrogen flow in the range of 773-1073 K.

The thermodynamics of ferrocene decomposition and hydrogenolysis were analyzed using the method described in [25–27], based on temperature dependences of the standard Gibbs free energy $\Delta G°_T$ and the equilibrium constant K_p. Thermodynamic parameters of all stable species were taken from [28]. Since reliable data for

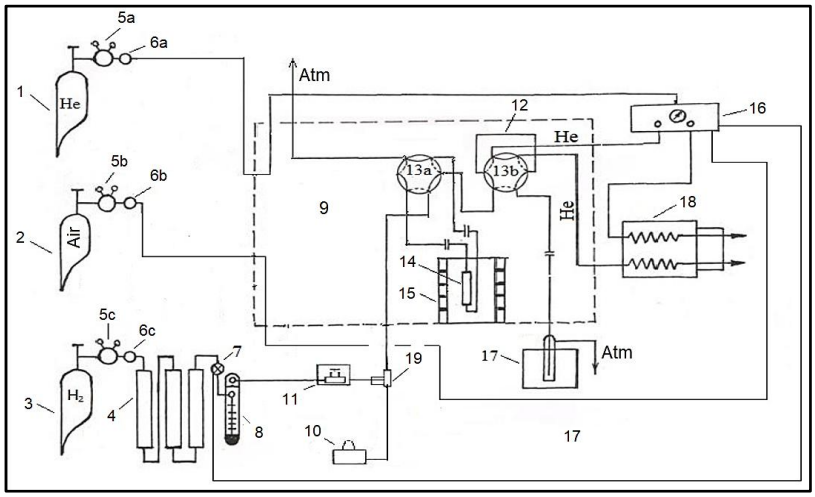

Fig. 1. Schematic diagram of the experimental laboratory setup used to carry out the ferrocene reduction reaction. Here: 1 – Helium cylinder; 2 – Air cylinder; 3 – Hydrogen cylinder; 4 – Columns for hydrogen gas purification; 5a, 5b and 5c – Two-chamber reducer; 6a, 6b and 6c – Low pressure regulator; 7 – Sensitive gas control valve; 8 – Capillary rheometer; 9 – Thermostate; 10 – Microsyringe pump; 11a and 11b – Valve; 12 – Sampling loop; 13a and 13b – Six-way valves; 14 – Reactor; 15 – Electric furnace; 16 – Chromatographic gas preparation unit; 17 – Reaction product collector; 18 – Chromatograph; 19 – Three-way control line for feeding gaseous hydrogen and feed mixture into the system.

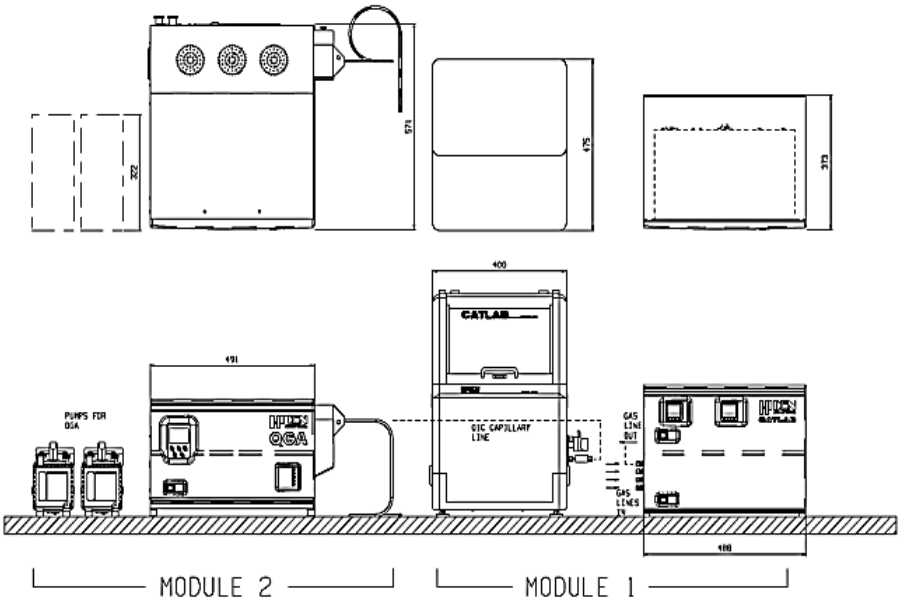

a)

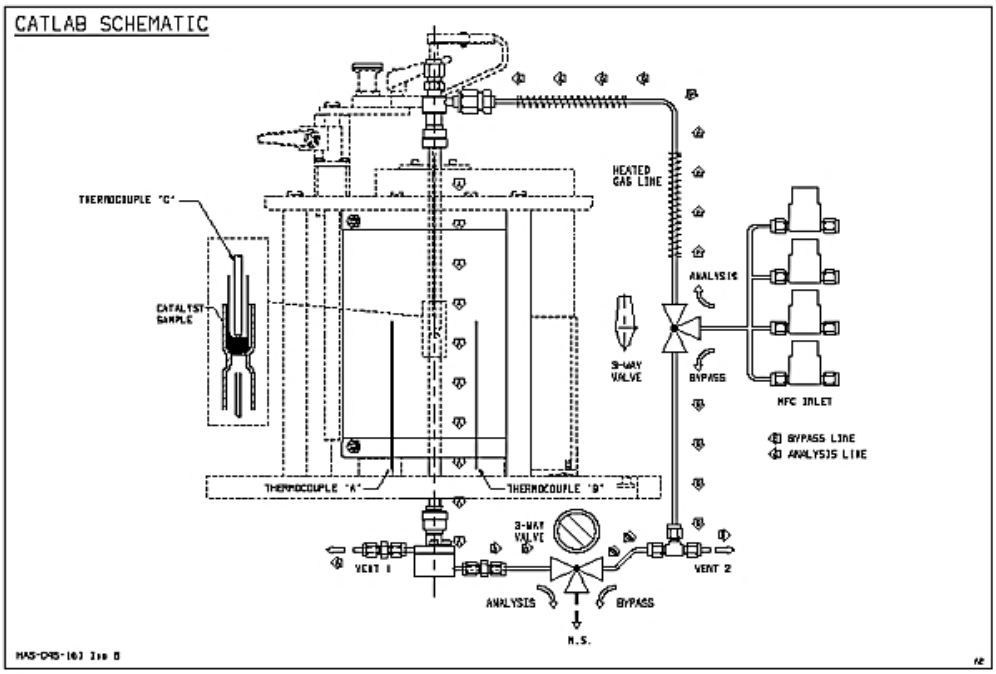

b)

Fig. 2. a, b General view (a) and schematic diagram (b) of the Catlab complex from Hiden Analytical Ltd., UK, which is a microreactor coupled with a mass spectrometer [24].

Table 1.

Relative content of gas-phase products of the reaction of thermal decomposition of ferrocene in a hydrogen flow at 773-1073K (Reaction conditions: $V(H_2)$ = 15 ml/min, m(ferrocene) = 0.3g)

S/N	T, K	Relative content, %						
		Methane	Ethane	n-Propane	n-Butane	n-Pentane	n-Hexane	dcp*
1.	773	5.5	2.5	3.2	4.3	43.3	38.1	3.1
2.	873	12.8	6.3	4.9	4.3	42.6	28.0	1.1
3.	973	41.9	32.8	13.1	8.8	1.9	1.2	0.3
4.	1073	58.6	24.6	12.9	2.2	0.9	0.6	<0.2

*dcp – dicyclopenthadien

gaseous dicyclopentadienyl ($C_{10}H_{10}$,g) are absent in the literature, its properties were estimated from the thermodynamic parameters of cyclopentadiene and the C–H bond dissociation and C–C bond formation energies [29]. The resulting values are:

$\Delta H^0_{298}(C_{10}H_{10},g)$= 734 kJ/mol;

$S^0_{298}(C_{10}H_{10},g)$= 235 J/ mol·K;

$C^0_{p,298}(C_{10}H_{10},g)$= 201 J/ mol·K.

For the overall pyrolysis reaction of ferrocene:

$$(C_5H_5)_2Fe(g) \rightarrow Fe\ (s) + CH_4(g) + C_2H_4\ (g) + C_2H_2\ (g) + 5C\ (s)$$

The calculated temperature dependences of $\Delta G°_T$ and $\ln K_p$ show that decomposition into iron, carbon and light hydrocarbons is thermodynamically more favorable. The formation of $C_{10}H_{10}$ as an intermediate is characterized by positive $\Delta G°_T$ over a wide temperature range, so the mechanism via dicyclopentadienyl is unlikely. Thus, ferrocene pyrolysis proceeds predominantly through direct decomposition to Fe, C and small hydrocarbons, rather than via a dicyclopentadienyl stage.

Comparison of the Gibbs free energies for reactions describing hydrogen-assisted decomposition indicates that increasing the hydrogen content promotes almost complete reduction of ferrocene. The reaction of ferrocene with hydrogen, leading to iron and cyclopentadiene, involves a solid–gas phase transition and is endothermic ($\Delta H > 0$) with a decrease in entropy ($\Delta S < 0$). Under standard conditions ΔG is positive, so the reaction is not spontaneous and requires external energy input. As temperature increases, $-T\Delta S$ becomes more significant, $\Delta G°_T$ decreases and K_p increases, but at moderate temperatures the equilibrium still remains shifted towards the initial ferrocene-containing state.

Using the calculated values of ΔH and ΔS, the critical temperature at which $\Delta G°_T = 0$ for the decomposition of ferrocene in a hydrogen stream is about 893 K. Above this temperature $\Delta G°_T$ becomes negative and the reaction is thermodynamically favorable. Therefore, efficient thermal decomposition and reduction of ferrocene to iron and volatile hydrocarbons require elevated temperatures ($T > 893$ K), while at lower temperatures the process is thermodynamically hindered and proceeds only upon sufficient external heating.

Figure 3, a, b show the X-ray diffraction pattern (a) and the FMR spectrum (b) of the solid product of thermal decomposition of ferrocene.

The presented X-ray diffraction pattern and FMR spectrum are characteristic of samples containing iron-carbon nanoparticles [30–32]. These peaks correspond to the characteristic reflections of the metallic iron phase (PDF #06-0696 (bcc structure)) and the iron carbide phase Fe_3C (PDF #35-0772 (orthorhombic structure)). In the sample obtained as a result of processing, the peak at 44.7° corresponds to the reflection (110) of bcc iron with a grain size of 11 nm (calculated using the Scherrer equation), while the intense peak at 43.4° with a grain size of 8 nm may correspond to the reflection (210) of Fe_3C. The results indicate the existence of individual Fe and Fe–C nanoparticles in the sample. It should be noted that the Fe–C phases are metastable phases and can decompose into Fe and C residues at high temperature. The diffraction pattern shows peaks with the Miller indices: for iron (Fe): (110), $2\theta \approx 44.7°$; (200), $2\theta \approx 65.0°$; (211), $2\theta \approx 82.5°$ and iron carbide (Fe_3C): (021), $2\theta \approx 37.8°$; (210), $2\theta \approx 43.4°$; (002), $2\theta \approx 78.5°$. Refined analysis using the Williamson–Hall method shows that the crystallite sizes of the Fe and Fe_3C phases are 10.95 nm and 8.49 nm, respectively, while the corresponding microstrain values amount to 2.03×10^{-4} for Fe and 1.11×10^{-3} for Fe_3C (details of the calculations are provided in Appendix 1).

In addition to X-ray diffraction studies, solid products of thermal decomposition of ferrocene were also studied using the ferromagnetic resonance (FMR) method. The FMR spectrum obtained at room temperature and shown in Fig. 6b is a superposition of FMR signals from iron nanoparticles, iron carbide Fe_3C, and amorphous carbon. Using the Landau-Lifshitz-Gilbert equation, the spectra were calculated depending on the composition of the sample and the size of the iron nanoparticles, iron carbide, and amorphous carbon. By comparison, the calculated FMR spectra were adjusted to the experimental one [33].

Thermal decomposition of ferrocene: As the temperature increases, ferrocene $Fe(C_5H_5)_2$ begins to decompose, releasing iron atoms and hydrocarbon radicals. This decomposition occurs at temperatures above 400-500 °C and can be described by the following

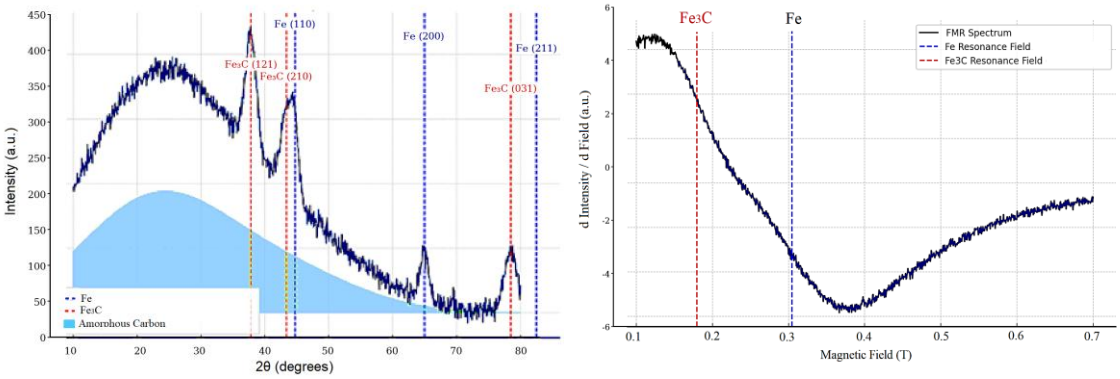

a) b)

Fig. 3, a, b. X-ray diffraction pattern (a), and the FMR spectrum (b) of the solid product of thermal decomposition of ferrocene. In (a) blue dashed lines: peak positions for Fe, red dashed lines: peak positions for Fe_3C and green shaded area: contribution from amorphous carbon; in (b) blue dashed lines: Fe nanoparticles resonance field and red dashed lines: Fe_3C nanoparticles resonance field.

reaction: $Fe(C_5H_5)_2 \rightarrow Fe+2C_5H_5^{\bullet}$. Ferrocene molecules lose stability at high temperatures, and the bonds between the iron atom and the cyclopentadienyl rings (C_5H_5) are broken. As a result of decomposition, iron atoms (mainly in the form of atomic or cluster iron) and hydrocarbon radicals $C_5H_5^{\bullet}$ are formed. The released iron atoms are highly active and easily aggregate at high temperatures, forming clusters. This process includes a nucleation stage:

at a certain concentration of iron atoms in the gas phase, they begin to spontaneously combine into nuclei (small clusters). When nuclei collide with iron atoms, the clusters begin to increase in size. This process involves both iron atoms and small iron clusters, which combine to form larger aggregates. These stages can be described as follows:

$$Fe_{atom}+Fe_{atom}\rightarrow Fe_2(\text{formation of small clusters})\ Fe_n+Fe_{атом}\rightarrow Fe_{n+1}(\text{cluster growth}).$$

The cluster growth process continues until nanoparticles of a certain size are stabilized. The particle size is determined by parameters such as temperature, pressure in the reaction chamber, and concentration of iron atoms in the gas phase. As the clusters reach a certain size, they become more stable and less susceptible to merging. At this stage, the nanoparticles are cooled. As the temperature decreases or the nanoparticles are removed from the reaction zone, their kinetic energy decreases, which prevents further particle merging. Under certain conditions, the surface of the nanoparticles can be stabilized by adsorption of hydrocarbon residues formed during the decomposition of ferrocene. These carbon residues can create a protective shell that prevents the aggregation of the nanoparticles. As a result, iron nanoparticles with a carbon shell are obtained at the output, which can serve as a passivation layer preventing oxidation and adhesion of the particles. This carbon layer can be amorphous carbon or a graphite-like structure, depending on the synthesis conditions.

Thermal decomposition of ferrocene can also produce by-products such as: carbon nanostructures (e.g. amorphous carbon or graphite) due to polymerization and pyrolysis of hydrocarbon radicals $C_5H_5^{\bullet}$, and iron oxide nanoparticles (if the process occurs in the presence of oxygen or when exposed to atmospheric air).

The final mechanism can be represented by the following stages:

1. Destruction of the ferrocene molecule under the influence of high temperature with the release of iron atoms and hydrocarbon radicals.

2. Condensation of iron atoms with the formation of clusters and their growth to nanosized particles.

3. Stabilization of nanoparticles with the possible formation of a carbon shell around them. Thus, thermal decomposition of ferrocene is a convenient method for synthesizing iron nanoparticles, since it allows you to obtain particles of the desired size with a carbon shell that protects them from oxidation.

The formation of iron nanoparticles during the thermal decomposition of ferrocene can be described by a sequence of kinetically and thermodynamically coupled stages: (1) dissociation of ferrocene molecules, (2) condensation (nucleation and growth) of iron atoms, and (3) growth of stable clusters into nanoparticles.

1. Dissociation of ferrocene

Assume that ferrocene decomposes according to $Fe(C_5H_5)_2 \rightarrow Fe + 2C_5H_5$.

The decomposition of ferrocene is treated as a first-order process:

$$d[Fe(C_5H_5)_2]/dt = -k_d[Fe(C_5H_5)_2],$$

where $[Fe(C_5H_5)_2]$ is the concentration of ferrocene and k_d is the decomposition rate constant at a given temperature.

The solution to this differential equation gives: $[Fe(C_5H_5)_2](t) =[Fe(C_5H_5)_2]_0e^{-k_dt}$, where $[Fe(C_5H_5)_2]_0$ - initial concentration of ferrocene.

The rate of formation of iron atoms is proportional to the decomposition rate:

$$d[Fe]/dt=k_d[Fe(C_5H_5)_2]$$

2. Condensation, nucleation and growth of iron clusters.

The iron atoms produced then condense to form clusters. This process is described in terms of nucleation and subsequent growth. The nucleation rate r_J is determined as follows:

$$r_J = A\cdot\exp(-\Delta G^*/k_BT).$$

where: A is the pre-exponential factor (depends on the concentration and kinetics of atoms), $\Delta G*$ is the free activation energy of nucleation (depends on the surface energy of the cluster), k_B is the Boltzmann constant, T is the temperature.

The free activation energy of nucleation ΔG^* can be approximately expressed through the surface energy γ of the cluster and its critical radius $r*$:

$$\Delta G^*=16\pi\gamma^3/3(\Delta G_v)^2,$$

where: γ is the surface energy of the cluster, ΔG_v is the change in free energy per unit volume during condensation.

Cluster growth occurs via attachment of iron atoms. Let a cluster contain n iron atoms. Its growth rate can be written as:

$$dn/dt=k_g[Fe]$$

where: k_g is the cluster growth rate constant, [Fe] is the concentration of iron atoms. Then the mass of a cluster M containing n iron atoms is determined as: $M=n\cdot m_{Fe}$, where m_{Fe} is the mass of one iron atom.

To relate the concentration of iron atoms and clusters, consider the balance of atoms in the system. Let N be the concentration of clusters, then the change in the concentration of iron atoms will be determined by the

relationship:

$$d[Fe]/dt = -k_g[Fe]\cdot N - k_d[Fe(C_5H_5)_2],$$

where: - $k_g[Fe]\cdot N$ – the rate of consumption of iron atoms for cluster growth, $-k_d[Fe(C_5H_5)_2]$ – the rate of decomposition of ferrocene molecules.

As the clusters grow, they reach a certain size at which they become stable nanoparticles. The average radius of nanoparticles R can be estimated based on the total number of iron atoms and the concentration of clusters. The average radius of nanoparticles is defined as:

$$R = (3M/4\pi\rho N)^{1/3},$$

where: M is the total mass of iron in the system, ρ is the density of iron, N is the concentration of clusters.

Thus, to model the process of condensation and growth of iron nanoparticles, the following differential equations can be used:

For the decomposition of ferrocene:

$$d[Fe(C_5H_5)_2]/dt = -k_d[Fe(C_5H_5)_2]$$

To concentrate iron atoms:

$$d[Fe]/dt = k_d[Fe(C_5H_5)_2] - k_g[Fe]\cdot N$$

For cluster (nanoparticle) growth:

$$dn/dt = k_g[Fe]$$

For the number of clusters:

$$dN/dt = r_J - k_g[Fe]\cdot N.$$

Below are the results of the numerical solution for determining the concentration of iron atoms and cluster growth over time.

Fig. 4 shows how the concentrations of ferrocene, iron atoms, and clusters change over time, as well as the evolution of cluster size during the condensation of iron produced by ferrocene decomposition.

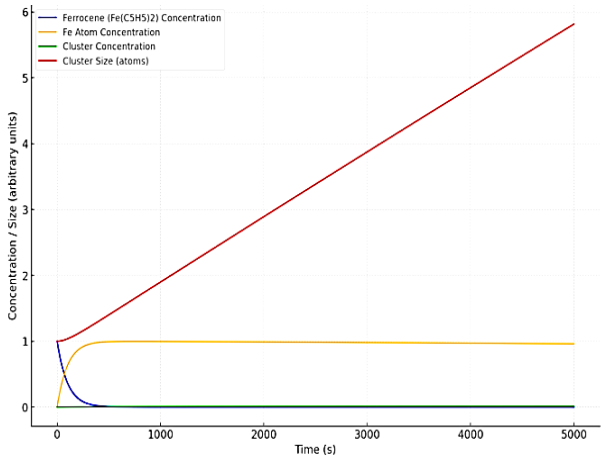

Fig. 4. Evolution of the concentrations of ferrocene molecules, iron atoms and clusters over time, as well as the size of the clusters (the number of atoms in each cluster) during the condensation of iron atoms formed as a result of the thermal decomposition of ferrocene.

Thus, the given figure allows us to establish the following:

1. Over time, the concentration of ferrocene (blue line) decreases exponentially as it degrades at a constant rate.
2. As ferrocene degrades, the concentration of iron atoms (orange line) increases rapidly but then reaches saturation. This is because iron atoms are used for cluster growth.
3. Nucleation and cluster growth (green line) occurs slowly as the cluster concentration remains low due to the limited growth rate and consumption of iron atoms.
4. Average cluster size (in terms of number of atoms) (red line): increases continuously as iron atoms are added to the clusters, causing them to continuously increase in size.

This result demonstrates the dynamic behavior of the iron nanoparticle formation process, starting from the decomposition of ferrocene molecules and ending with the growth of clusters to nanoscale sizes.

Fig. 5a,b shows the time evolution of cluster (particle) size, expressed as the number of atoms per cluster, in a) linear and b) nonlinear (exponential) forms."

The numerical solution procedure for this system of differential equations consisted of: We set the initial concentrations and rate parameters for the simulation: The rate constant of ferrocene decay (k_d) is the rate at which ferrocene molecules decompose into iron atoms. The rate constant of cluster growth (k_g) determines the rate at which iron atoms attach to clusters. The nucleation rate (r_J) determines the initial concentration of clusters (nucleation).

The system of differential equations below describes the kinetics of the process of formation and growth of iron clusters:

Decomposition of ferrocene:

$$d[Fe(C_5H_5)_2]/dt = -k_d[Fe(C_5H_5)_2]$$

Concentration of iron atoms:

$$d[Fe]/dt = k_d[Fe(C_5H_5)_2] - k_g[Fe]\cdot[clusters]$$

Concentration of clusters:

$$d[clusters]/dt = r_J - k_g[Fe]\cdot[clusters]$$

Cluster size (number of atoms in a cluster):

$$dn/dt = k_g[Fe]$$

For the numerical solution, the initial conditions are set for each variable: $[Fe(C_5H_5)_2]_0$ is the initial concentration of ferrocene molecules. $[Fe]_0=0$ is the initial concentration of iron atoms (there are no atoms before the decay of ferrocene), $[clusters]_0=0$ is the initial concentration of clusters, $n_0=1$ is the initial cluster size (the minimum number of atoms). The Runge-Kutta method was used to numerically solve the system of differential equations. The solution specifies the time range and steps for integration. The code for the numerical solution is given in Appendix 2. This code was used to plot the graphs shown in Fig. 5.

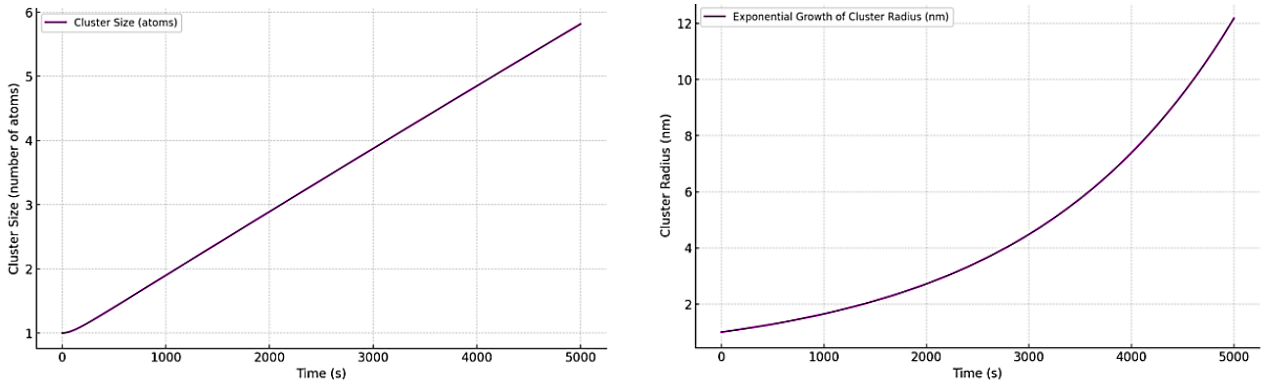

a) b)

Fig. 5, a, b. Dynamics of the cluster (particle) size over time, represented by the number of atoms in each cluster in: a) linear, b) nonlinear (exponential) versions.

The graph above shows the dynamics of the cluster (particle) size over time, represented by the number of atoms in each cluster.

As can be seen from Fig. 5,a, the cluster size increases linearly with time, indicating continuous growth as more and more iron atoms are combined into clusters. This steady growth suggests that iron atoms are readily available for cluster growth, and the aggregation rate remains relatively stable during the observed period. However, this linear growth trend will eventually slow down under real conditions as the concentration of iron atoms decreases or if additional stabilizing factors begin to affect the system.

It should be noted that cluster growth can be nonlinear. The nonlinearity of growth is usually associated with various factors affecting the condensation and aggregation process of atoms. In Figure 5b shows the exponential growth of the iron cluster radius (in nanometers) as a function of time. The cluster radius grows exponentially with time, which is typical for cases where the conditions favor a constant acceleration of growth. This can occur, for example, at high supersaturation, when the concentration of iron atoms remains high and does not limit growth. Such exponential growth is rarely observed in real conditions, since limiting factors such as a decrease in the atomic concentration and diffusion limitations usually come into play over time. Thus, cluster growth is often nonlinear due to a combination of factors such as changes in atomic concentration, diffusion limitations, coalescence, surface passivation, and energy barriers. Linear growth is observed only under limited conditions, when external factors have little effect on the process, or at the initial stages of growth, when the atomic concentration is still quite high, and diffusion and passivation limitations do not play a significant role.

Below is a mathematical description of the dependence of the critical nucleus radius on the free energy of the system. Consider a spherical droplet of radius r, which is formed from a supersaturated vapor or solution. The free energy of the nucleus G(r) consists of two main contributions: The critical radius of the nucleus is the minimum size of the cluster at which it becomes thermodynamically stable and can continue to grow. Nuclei smaller than the critical radius tend to disintegrate, while those larger than the critical radius tend to grow further. The critical radius depends on the free energy of the system and can be determined based on the ratio of the surface and volume free energies of the nucleus. Since condensation reduces the free energy of the system, the volume free energy ΔG_v is negative. The surface energy γ is positive, since the formation of a new surface requires energy. The free energy of the nucleus G(r) can be written as the sum of the volume and surface energies:

$$G(r)= (4/3)\pi r^3\Delta G_v+4\pi r^2\gamma,$$

where: ΔG_v is the change in free energy per unit volume (usually negative), γ is the surface energy per unit area (positive value), r is the cluster radius.

To determine the critical radius r^*, it is necessary to determine the radius at which the free energy G(r) reaches its maximum. To do this, we differentiate G(r) with respect to r and equate the derivative to zero:

$$dG(r)/dr = 4\pi r^2\Delta G_v+8\pi r\gamma =0.$$

Solving this equation for r, we obtain: $r^* = -2\gamma\Delta G_v$, where: r^* is the critical radius, γ is the surface energy, ΔG_v is the change in free energy per unit volume (usually negative during condensation). Since ΔG_v is negative, r^* will be positive. If the radius of the nucleus $r<r^*$, then its free energy G(r) increases, and such nuclei tend to disintegrate. If the radius of the nucleus $r>r^*$, then the free energy G(r) decreases with increasing radius, and the nucleus will grow, since the process becomes energetically favorable. The volumetric free energy ΔG_v depends on the degree of supersaturation S in the system. The greater the supersaturation, the stronger the driving force for the formation of nuclei, and the smaller r^* will be. In the case of vapors or solutions, the degree of supersaturation can be related to the concentration or pressure of the system. $\Delta G_v=-k_BTlnS$. Then the critical radius can be rewritten as: $r*=2\gamma k_BTlnS$, where: k_B is the Boltzmann constant, T is the temperature, S is the degree of supersaturation (the ratio of the current concentration to the equilibrium concentration). Thus, it can be concluded that the critical radius r^* is inversely proportional to the supersaturation S and directly proportional to the surface energy γ. At high supersaturation S, the critical radius

decreases, which facilitates the formation of stable nuclei.

In an inert atmosphere, the surface energy of iron is usually about $\gamma_{inert} \approx 2$ J/m^2. In a hydrogen atmosphere, γ can change due to hydrogen adsorption on the surface, which reduces the surface energy. For an estimate, we can take the value $\gamma(H_2) \approx 1.5$ J/m^2. The change in volumetric free energy per unit volume can be expressed as: $\Delta G_v = -k_B T \ln S$, where: k_B is the Boltzmann constant (1.38×10^{-23} J/K), T is the temperature in kelvins, and S is the degree of supersaturation. For an estimate, we choose a temperature of about T=1000 K, which is typical for the thermal decomposition of ferrocene, and a degree of supersaturation S=10 (which corresponds to moderate supersaturation).

For inert gas:

$$\Delta G_v = -k_B T \ln S = -(1.38 \times 10^{-23}) \times 1000 \times \ln(10) \approx -3.18 \times 10^{-21} \text{ J}$$

$$r_{inert}^* = \frac{-2 \times 2 \text{ J/m}^2}{-3.18 \times 10^{-21} \text{ J}} \approx 1.26 \times 10^{-9} \text{ m} = 1.26 \text{ nm}$$

For hydrogen:

$$r_{H2}^* = \frac{-2 \times 1.5 \text{ J/m}^2}{-3.18 \times 10^{-21} \text{ J}} \approx 0.94 \times 10^{-9} \text{ m} = 0.94 \text{ nm}$$

Thus, it can be concluded that in an inert atmosphere, the critical radius of the nucleus for iron particles is approximately $r_{inert}^* \approx 1.26$ nm. In a hydrogen atmosphere, the critical radius decreases and is $r(H_2)^* \approx 0.94$ nm. In a hydrogen atmosphere, the critical radius is smaller than in an inert atmosphere. This is due to the fact that hydrogen is adsorbed on the surface of iron particles, reducing the surface energy γ, which facilitates the formation of stable nuclei of smaller size. Thus, the formation of iron nanoparticles during thermal decomposition of ferrocene will occur with smaller sizes of nuclei in a hydrogen atmosphere, which can contribute to more intense formation and growth of nanoparticles.

Conclusion

Ferrocene is currently one of the most widely used precursors in the synthesis of carbon nanotubes (CNTs), iron-containing catalysts with a controlled size of the active component. To control the composition of the products, it is necessary to understand the mechanism of ferrocene decomposition under various reaction conditions. Intermediate compounds act either as a stimulator of CNT growth, serve as carbon raw materials, or as a harmful impurity, reducing the growth rate due to the formation of undesirable volatile and polyaromatic hydrocarbons that deactivate iron particles acting as a catalyst. When decomposing ferrocene in a hydrogen atmosphere, it is important to maintain a constant temperature and hydrogen feed rate to control the degree of hydrogenation of the thermal decomposition products and thereby control the size and structure of the resulting nanomaterials. To build a mechanism for the thermal decomposition of ferrocene in a hydrogen stream, the key reaction stages and experimental methods that can be used to confirm the formation of products are considered. This process can be used to obtain various nanomaterials and catalytic systems based on iron and carbon. Depending on the composition of the phase formed, different growth modes of Fe nanoparticles arise under the influence of hydrocarbons. Our results show that the composition of the gas-phase and solid products of thermal reduction of ferrocene depends significantly on the conditions of the thermal decomposition reaction and in this context the chemistry of thermal decomposition of ferrocene requires the involvement, first of all, in situ combination of chromato-mass-spectrometry methods with X-ray structural, optical and magnetic resonance spectroscopy.

Acknowledgments

The work was carried out with the financial support of the Ministry of Science and Education of the Azerbaijan Republic "Research and development in priority areas of catalysis and industrial chemistry. Preparation of oxide and polymer-based nanostructured catalysts, adsorbents and nanostructures."

Appendix 1. Calculations details of the crystallite size and microstrain values.

The crystallite size and microstrain values were calculated using the Williamson-Hall equation:

$\beta \cdot \cos(\theta) = (K \cdot \lambda / D) + 4 \cdot \epsilon \cdot \sin(\theta)$,

where

β is the peak half-width (FWHM) in radians, θ is the Bragg angle in radians,

K is the shape factor (usually taken to be 0.9 for spherical particles)

λ is the X-ray wavelength (for CuK_α is 0.15406 nm),

D is the crystallite size,

ϵ is the microstrain.

Calculation steps

Step 1. Determine the peak half-width (β) and Bragg angles (θ).

Initial data for the iron phase:

$2\theta_1(Fe) = 44.7°$, $2\theta_2 = 65.0°$, $2\theta_3 = 82.5°$;

Half-widths: $\beta_1 = 0.8°$, $\beta_2 = 0.9°$, $\beta_3 = 1.0°$

Converting them to radians

$\beta(\text{rad}) = \beta \times (\pi/180)$

$\theta(\text{rad}) = (2\theta/2) \times \pi/180)$

Step 2. Plot a graph of $\beta \cdot \cos(\theta)$ versus $\sin(\theta)$.

Step 3. Perform a linear regression using the equation: $y = kx + b$

Where:

$y = \beta \cdot \cos(\theta)$,

$x = \sin(\theta)$,

The slope (k) gives 4ϵ,

The y-intercept (b) is used to estimate the crystallite size

Step 4. Calculate the microstrain: $\epsilon = (k/4)$.

Step 5. Calculate the crystallite size (D) from the b-intercept: $D = K \cdot \lambda / b$

Calculation example

For the first line:

$\beta_1 = 0.8^\circ = 0.01396$ rad, $\theta 1 = 22.35^\circ = 0.3899$ rad.

Calculate:

$\beta_1 \cdot \cos(\theta 1) = 0.01396 \cdot \cos(0.3899) \approx 0.0130$

$\sin(\theta_1) = \sin(0.3899) \approx 0.3800$

After performing linear regression on all data, we get:

k=0.000812, which gives $\epsilon = (0.000812/4) = 2.03 \times 10-4$,

Intercept b=0.0140, which corresponds to $D=0.9 \times 0.154060.0140 \approx 10.95$ nm

Appendix 2. Code for numerical calculations and plotting of graphs in Fig. 5.

```
python
import numpy as np
from scipy.integrate import solve_ivp
import matplotlib.pyplot as plt

# Constants
k_d = 0.01  # Dissociation rate constant of ferrocene (s^-1)
k_g = 0.001  # Growth rate constant of clusters (s^-1)
J = 1e-5  # Nucleation rate (clusters/s)

# Initial conditions
initial_FeC5H5 = 1.0  # Initial concentration of ferrocene (arbitrary units)
initial_Fe = 0.0  # Initial concentration of Fe atoms (arbitrary units)
initial_clusters = 0.0  # Initial concentration of clusters (arbitrary units)
initial_n = 1.0  # Initial number of atoms in a cluster (small seed)

# Define the system of differential equations
def system(t, y):
    FeC5H5, Fe, clusters, n = y
    d_FeC5H5_dt = -k_d * FeC5H5  # Dissociation of ferrocene
    d_Fe_dt = k_d * FeC5H5 - k_g * Fe * clusters  # Change in Fe concentration
    d_clusters_dt = J - k_g * Fe * clusters  # Growth of clusters (number of clusters)
    d_n_dt = k_g * Fe  # Growth of cluster size (atoms in a cluster)
    return [d_FeC5H5_dt, d_Fe_dt, d_clusters_dt, d_n_dt]

# Time span for the simulation
time_span = (0, 5000)  # Simulation time in seconds
initial_conditions = [initial_FeC5H5, initial_Fe, initial_clusters, initial_n]

# Solve the system of differential equations
solution = solve_ivp(system, time_span, initial_conditions, method='RK45', t_eval=np.linspace(0, 5000, 1000))

# Extract results
t = solution.t
FeC5H5_concentration = solution.y[0]
Fe_concentration = solution.y[1]
clusters_concentration = solution.y[2]
cluster_size = solution.y[3]

# Plotting results
plt.figure(figsize=(12, 8))
plt.plot(t, FeC5H5_concentration, label="Ferrocene (Fe(C5H5)2) Concentration", color='blue')
plt.plot(t, Fe_concentration, label="Fe Atom Concentration", color='orange')
plt.plot(t, clusters_concentration, label="Cluster Concentration", color='green')
plt.plot(t, cluster_size, label="Cluster Size (atoms)", color='red')
plt.xlabel("Time (s)")
plt.ylabel("Concentration / Size (arbitrary units)")
plt.title("Time Evolution of Iron Atom Concentration and Cluster Growth")
plt.legend()
plt.grid(True)
plt.show()
```

Rustamova A.I. *– Dr., Assoc. Prof. leading researcher;*
Huseynova L.V. *– Dr., Assoc. Prof.;*
Osmanova S.N. *– Dr., leading researcher;*
Ahmadov V.M. *– Dr., Senior Researcher;*
Ismailov E.H. *– Dr. Sc. Chem., Prof., Head of Laboratory.*

[1] H. Werner, *At least 60 years of ferrocene: the discovery and rediscovery of the sandwich complexes*. Angewandte Chemie, 51 (25), 6052 (2012); https://doi.org/10.1002/anie.201201598.
[2] E.S. Phillips, *Ferrocenes. compounds, properties and applications*. Chemical engineering methods and technology (Nova Science Publishers, 2011).
[3] S. Islam and F. Wang, *A comparative study of energetics of ferrocenium and ferrocene*, Preprints, 1, (2018); https://doi.org/10.20944/preprints201808.0166.
[4] Ya-Ru Deng, Ya-Fei Li, Hao Yang, Yan-Ru Fan, Yu Huang, Synthesis, DNA binding of bis-naphthyl ferrocene derivatives and the application as new electroactive indicators for DNA biosensor, Journal of Inorganic Biochemistry, 257, (112615), (2024); https://doi.org/10.1016/j.jinorgbio.2024.112615.

[5] Woojung Lee, Liang Li, María Camarasa-Gómez, Daniel Hernangómez-Pérez, Xavier Roy, Ferdinand Evers, Michael S. Inkpen, Latha Venkataraman, *Photooxidation driven formation of Fe-Au linked ferrocene-based single-molecule junctions*, Nature Communications, 15, 1, (2024); https://doi.org/10.1038/s41467-024-45707-z.

[6] Y.Y. Zhuk, N.G. Strizhakova, & Y.A. Maletin, *Ferrocene-containing ligands in the self-assembly of trinuclear μ_3-oxocentered carboxylate complexes of chromium (III, III, III)carboxylate complexes of chromium(III, III, III).* Theor Exp Chem, 36, 215 (2000); https://doi.org/10.1007/BF02522754.

[7] Abeera Hassan, Hafiza Komal Zafar, Ayman Nafady, Manzar Sohail, *Synthesis and characterization of novel ferrocene/PbS nanocomposite material by low-temperature co-precipitation method*, Inorganic Chemistry Communications, 162, 112194 (2024); https://doi.org/10.1016/j.inoche.2024.112194.

[8] Umair Rauf, Ghulam Shabir, Saba Bukhari, Fernando Albericio, Aamer Saeed, *Contemporary Developments in Ferrocene Chemistry: Physical, Chemical, Biological and Industrial Aspects*, Molecules, 28(15), 5765 (2023); https://doi.org/10.3390/molecules28155765.

[9] Mingli Xu, Chen Wu, Fengxue Zhang, Yanhui Zhang, Jiaxin Ren, Chengyi Zhang, Xuanze Wang, Li Xiao, Olivier Fontaine, Jiangfeng Qian, *Potential regulation strategy enables ferrocene as p-type redox mediator for direct regeneration of spent $LiFePO_4$ cathode*, Energy Storage Materials, 71, 103611 (2024); https://doi.org/10.1016/j.ensm.2024.103611.

[10] F.A. Larik, A. Saeed, T.A. Fattah, U. Muqadar, P.A. Channar, *Recent advances in the synthesis, biological activities and various applications of ferrocene derivatives,* Appl. Organomet. Chem. 31, 3664 (2017); https://doi.org/10.1002/aoc.3664.

[11] Noha A. Elessawy, Mohamed Elnouby, M.H. Gouda, Hesham A. Hamad, Nahla A. Taha, M. Gouda, Mohamed S. Mohy Eldin. *Ciprofloxacin removal using magnetic fullerene nanocomposite obtained from sustainable PET bottle wastes: Adsorption process optimization, kinetics, isotherm, regeneration and recycling studies.* Chemosphere, 239, 124728 (2020); https://doi.org/10.1016/j.chemosphere.2019.124728.

[12] Praswasti PDK Wulan, Togi Elyazeer Sinaga. *The effect of iron-carbon ratio and on carbon nanotube synthesis using camphor and ferrocene as carbon sources in the gauze reactor*. South African J. of Chem. Engineering, 36, 17 (2021); https://doi.org/10.1016/j.sajce.2020.12.001.

[13] Cameron H.W. Kelly, Matthias Lein. *Choosing the right precursor for thermal decomposition solution-phase synthesis of iron nanoparticles: tunable dissociation energies of ferrocene derivatives*. Physical Chemistry Chemical Physics, *18* (47), 32448(2016); https://doi.org/10.1039/C6CP06921E.

[14] Amlan Rooj, Madhusudan Roy, Ashis Bhattacharjee. *Thermal Decomposition Reaction of Ferrocene in the Presence of Oxalic Acid.* International Journal of Chemical Kinetics, 49(5), 319 **(2017);** https://doi.org/10.1002/kin.21077.

[15] Bo-Yu Chen, Chong-Chi Chi, Wen-Kuang Hsu, Hao Ouyang. *Synthesis of SiC/SiO_2 core–shell nanowires with good optical properties on $Ni/SiO_2/Si$ substrate via ferrocene pyrolysis at low temperature*. Scientific Reports 11 (1), (2021); https://doi.org/10.1038/s41598-020-80580-y.

[16] Aqeel Hussain, Kirill Murashko, Alexey P. Tsapenko, Er-Xiong Ding, Esko I. Kauppinen, Anna Lähde. *Single-Step Fabrication of Iron Single-Walled Carbon Nanotube Film from Ferrocene as a Conductive-Electrocatalyst Interlayer in Lithium–Sulfur Batteries.* The Journal of Physical Chemistry C, 127(49), 23577 (2023); https://doi.org/10.1021/acs.jpcc.3c05777.

[17] V.V. Ivanovskaya, A.L. Ivanovskii, *Quantum-chemical modelling of composite nanomaterials: Iron clusters Fe_n (n = 6, 15, 19) in carbon nanotubes*. Theor Exp Chem, 42, 239 (2006); https://doi.org/10.1007/s11237-006-0046-z.

[18] Matthys J. Loedolff, Rebecca O. Fuller, Gareth L. Nealon, Martin Saunders *Mark A. Spackman and George A. Koutsantonis. Solution-phase decomposition of ferrocene into wüstite-iron oxide core–shell nanoparticles*. Dalton Trans., 51, 1603 (2022); https://doi.org/10.1039/D1DT03222D.

[19] M. Ivantsov, K. Krysanova, A. Grabchak, & M. Kulikova, *Hydrogenation of CO in the Presence of Fe-Containing Materials Based on Carbon Supports*. Eurasian Chemico-Technological Journal, 24(4), 303 (2022); https://doi.org/10.18321/ectj1474.

[20] Ashis Bhattacharjee, Amlan Rooj, Debasis Roy, and Madhusudan Roy. *Thermal Decomposition Study of Ferrocene $[(C_5H_5)_2Fe]$*. Hindawi Publishing Corporation Journal of Experimental Physics, 513268 (2014); http://dx.doi.org/10.1155/2014/513268.

[21] Sani Kundu, Toton Sarkar, Gurupada Ghorai, Pratap K. Sahoo, Ahmad Aziz Al-Ahmadi, Ahmad Alghamdi, Ashis Bhattacharjee, *Reaction Atmosphere-Controlled Thermal Conversion of Ferrocene to Hematite and Cementite Nanomaterials-Structural and Spectroscopic Investigations*, ACS Omega, 9 (21), 22607 (2024); https://doi.org/10.1021/acsomega.3c10332.

[22] Sebastian Grimm, Patrick Hemberger, Tina Kasper, Burak Atakan. *Mechanism and Kinetics of the Thermal Decomposition of $Fe(C_5H_5)_2$ in Inert and Reductive Atmosphere: A Synchrotron-Assisted Investigation in A Microreactor*. Advanced Materials Interfaces, 9 (22), (2022); https://doi.org/10.1002/admi.202200192.

[23] Kazunori Kuwana, Kozo Saito. *Modeling ferrocene reactions and iron nanoparticle formation: Application to CVD synthesis of carbon nanotubes*. Proceedings of the Combustion Institute, 31(2), 1857 (2007); https://doi.org/10.1016/j.proci.2006.07.097.

[24] Web source: https://www.hiden.de/wp-content/uploads/pdf/CATLAB.pdf

[25] A.I. Rustamova, Z.G. Gurbanov, Z.M. Mammadova, et al., *Heteronuclear Fe-Mn Cyclopentadienyl Complexes Supported on Boehmite. Thermochemistry and Thermodynamics of their Decomposition*, Chemical Problems, 26(3), 251 (2023); https://doi.org/10.32737/2221-8688-2023-3-251-261.

[26] A.I. Rustamova, Z.M. Mammadova, S.N. Osmanova, et al., *Thermal stability of cyclopentadienyliron-manganese(cobalt)-carbonyl halides adsorbed on alumina and thermodynamics of their decomposition. Ukrainian Conference with International Participation,* Chemistry, Physics and Technology of Surface, Book of abstracts, 11-12 October, 2023, Kyiv, Ukraine. https://drive.google. com/file/d/1nBmxAKF9UJFWeEocCme5DTWkvW-50Jk8T/view.

[27] A. Rustamova, R. Muradxanov, S. Osmanova, F. Pashayeva, A. Mammadov, D. Tagiyev, & E. Ismailov, *Heteronuclear Fe-Mn Cyclopentadienyl Complexes Supported on Boehmite. Thermochemistry and Thermodynamics of their Decomposition*. Eurasian Chemico-Technological Journal, 26(3), 161 (2024); https://doi.org/10.18321/ectj1639.

[28] Brief Handbook of Physical and Chemical Quantities, edited by K.P. Mishchenko and A.A. Ravdel, L.: Chemistry, 1974 – 200 pp. https://studylib.ru/doc/6242384/kratkij-spravochnik-fiziko-himicheskih-velichin.-pod-red.

[29] William M. Haynes; David R. Lide; Thomas J. Bruno, eds. *CRC handbook of chemistry and physics: a ready-reference book of chemical and physical data* (2016-2017, 97th ed.). Boca Raton, Florida: CRC Press. (2016); https://tech.chemistrydocs.com/Books/Organic/Basic-Organic-Chemistry-for-the-Life-Sciences-by-Hrvoj-Van%C4%8Dik.pdf.

[30] Hafsa Khurshid, Yassir A. Abdu, Eamonn Devlin, Bashar Afif Issab and George C. Hadjipanayis. *Chemically synthesized nanoparticles of iron and iron-carbides*, RSC Adv, 10(48), 28958 (2020); https://doi.org/10.1039/d0ra02996c.

[31] C.T. Hseih, W.L. Huang, J.T. Lue, *The change from paramagnetic resonance to ferromagnetic resonance for iron nanoparticles made by the sol–gel method*. J. of Physics and Chemistry of Solids, 63, 733 (2002); https://doi.org/10.1016/S0022-3697(01)00222-0.

[32] K. Chalapat, JVI Timonen, M. Huuppola, L. Koponen, C. Johans, RHA Ras, O. Ikkala, MA Oksanen, Seppälä, E & GS Paraoanu, *Ferromagnetic resonance in ε-Co magnetic composites'*, Nanotechnology, 25(48), 485707 (2014); https://doi.org/10.1088/0957-4484/25/48/485707.

[33] F.F Orudzhev, N.M.-R Alikhanov, S.M. Ramazanov, D.S. Sobola, R.K. Murtazali, E.H.Ismailov, R.D. Gasimov, A.S. Aliev, Ş. Ţălu, *Morphotropic Phase Boundary Enhanced Photocatalysis in Sm Doped $BiFeO_3$*. Molecules. 27(20), 7029 (2022); https://doi.org/10.3390/molecules27207029.

А.І. Рустамова[1], Л.В. Гусейнова[2], С.Н. Османова[1,3], В.М. Ахмадов[1], Е.Х. Ісмаілов[1]

Вплив термічного відновлення у потоці H_2 на склад продуктів розкладу ферроцену

[1] Інститут каталізу та неорганічної хімії, м. Баку, Азербайджан;
[2] Азербайджанський державний університет нафти та промисловості, м. Баку, Азербайджан;
[3] Університет Хазар, м. Баку, Азербайджан, sevinj.nasib.osmanli.26@gmail.com

Досліджено газофазні та твердофазні продукти, що утворюються під час термічного відновлення ферроцену в потоці водню в інтервалі температур 373–1073 K. До ідентифікованих газофазних продуктів належать метан, етан, пропан, бутан, *n*-пентан, *n*-гексан та циклопентадієн, тоді як твердофазні продукти представлені нанорозмірними частинками заліза та вуглецю. Отримано температурні залежності вмісту виявлених газофазних продуктів. Показано, що утворення наночастинок заліза під час термічного розкладу ферроцену в атмосфері водню супроводжується формуванням металевого заліза, карбіду заліза та аморфного вуглецю, причому їхній вміст у твердих залишках істотно залежить від умов реакції. Встановлено, що в атмосфері водню процес зародження відбувається з утворенням ядер меншого розміру, що сприяє інтенсивнішому формуванню та росту наночастинок. Склад твердих залишків реакції термічного розкладу ферроцену може бути керовано змінений шляхом варіювання експериментальних умов — часу реакції, температури та концентрації залізовмісного прекурсору. Магнітні властивості твердих продуктів реакції також можуть модулюватися залежно від структури та фазового складу частинок.

Ключові слова: ферроцен, термічне відновлення, газофазні продукти, твердофазні продукти, залізо, наночастинки карбіду заліза, рентгеноструктурний аналіз (XRD), феромагнітний резонанс (FMR).